THESIS

EXPLORATION OF A GEOMETRIC APPROACH FOR ESTIMATING SNOW SURFACE ROUGHNESS

Submitted by

David Jeffrey Kamin

Department of Ecosystem Science and Sustainability

In partial fulfillment of the requirements

For the Degree of Master of Science

Colorado State University

Fort Collins, Colorado

Fall 2015

Master's Committee:

      Advisor: Steven R. Fassnacht

      John D. Stednick
      William Bauerle

ABSTRACT

EXPLORATION OF A GEOMETRIC APPROACH FOR ESTIMATING SNOW SURFACE ROUGHNESS

The roughness of a surface that influences atmospheric turbulence is estimated as the aerodynamic roughness length (Z_0), and is used to understand the flow of air, temperature, and moisture over a surface. Z_0 is a critical variable for estimating latent and sensible fluxes at the surface, but most land surface models treat Z_0 simply as a function of land cover and do not address the variability of this value, such as due to changing snow surfaces. This is due in large part to the difficulty and cost of obtaining reliable estimates of Z_0 under field conditions.

This work addresses the need for versatile methods to evaluate snow surface roughness on a plot-scale. This study used anemometric data from a meteorological tower near Fort Collins, Colorado over two winters (2013-2014). Thorough screening yielded 153 wind-speed profiles which were used to calculate the aerodynamic roughness length at different times and under different snow conditions. The anemometric Z_0 values observed in this study with changing surface conditions ranged by 2.5 orders of magnitude from 0.2 to 52 x 10^{-3}m. Concurrently, a terrestrial laser scanner was used periodically to measure surface geometry and generate point clouds across the study site. Point clouds were processed and interpolated onto a regular grid for estimation of Z_0 based on the geometry and distribution of surface roughness elements. Two different geometric evaluations, the Lettau and Counihan methods, were used for the estimation of Z_0. The estimates based on surface geometry were evaluated and

compared to anemometric Z_0 values calculated from field observations of wind turbulence across the surface of the study site.

The Lettau method Z_0 values compared well to the measured anemometric results, with low but acceptable Nash-Sutcliffe Efficiency Coefficient (NSE) of 0.14 and a strong coefficient of determination (R^2 = 0.90). While the NSE was small, the Lettau Z_0 values could easily be scaled to the anemometric Z_0. The Counihan method yielded less accurate results compared to the anemometric data, with a NSE of -1.1. The data also showed a strong correlation between Z_0 and changing snow cover. The coefficient of determination between Z_0 and snow-covered area for both the anemometric and Lettau methods was greater than 0.7, indicating that both methods responded well to changing surface conditions.

ACKNOWLEDGEMENTS

TABLE OF CONTENTS

1. INTRODUCTION

In cold climates, the snow surface is often the interface between the atmosphere and the earth. The roughness of snow surfaces is an important control on air-snow heat transfer (Munro, 1989) and on the albedo of the snow surface (Warren, 1998). Since a seasonal snowpack can cover over 50% of the land area in the Northern Hemisphere (Mialon *et al.*, 2005), changes in the snow surface can have substantial effects on the Earth's energy budget. Thus it is crucial to understand the behavior of seasonal snow cover and its roughness properties.

The term "roughness" is sometimes used ambiguously. It is helpful to make a distinction between roughness as a property of a surface (surface or physical roughness) and roughness as a property of a flow (aerodynamic roughness length). The former is a combination of the vertical range and variability or irregularity of a surface. Aerodynamic roughness length in the field of fluid dynamics refers to the vertical distance from the boundary at which flow velocity equals zero. Roughness is often used as a synonym for flow resistance, and thus the calculated roughness is a property of a flow rather than the surface (Smith, 2014). This distinction will be explained further, but for this work "surface roughness" refers to the physical characteristics of the surface and "aerodynamic roughness" refers to the roughness length calculated from flow velocity profiles.

Snow is a complicated surface with rapidly evolving physical roughness characteristics. The atmospheric conditions under which snow falls and the metamorphism of snow crystals by temperature and wind affect micro-scale surface roughness. Melting and freezing processes

restructure the snowpack and snow surfaces over time. Topography and canopy also factor in to snowpack composition and surface characteristics. Canopy can affect snow water equivalent (SWE), depth, density, and distribution of snow (e.g., Winkler *et al*., 2005). Snow falling from branches and litter from the canopy can create depressions in the snow surface, and canopy and vegetation affect wind speeds and air temperatures. In open areas, wind is usually the dominant process affecting snow distribution (Lehning *et al*., 2008). All of these processes have the potential to affect the physical characteristics of the snow surface.

Until recently, the roughness of snow surfaces has not been well-studied (Lacroix *et al.,* 2008 has an overview of the history of measuring snow surface roughness). Measurements of snow surface roughness started in the 1980's with a black plate used as an arbitrary reference level to compare snow depth. This allowed for observations of millimeter-scale variations in snow surface features (Rott, 1984; Williams *et al*., 1988). Improvements have been made in accuracy using two-dimensional photography and digital processing (e.g. Fassnacht *et al*., 2009a), but this plate technique only provides information on roughness over short distances, and post-processing can be time-consuming and labor intensive. There are techniques and software for automating this plate technique (e.g. Manninen *et al.,* 2012) which allow for widespread use in different conditions but still cannot estimate surface roughness on a larger scale.

Methods based on laser scanning have recently been developed to measure snow surface characteristics. While initial efforts using near-surface laser scanning hardware have focused on snow depth (e.g. Deems *et al.* 2013), its application has expanded to measure other

characteristics of a snowpack such as surface roughness. The advantages of using such equipment include larger spatial coverage than plates and the generation of three-dimensional data sets. Satellite imaging and radar-based methods have excellent spatial coverage but lack resolution, with a typical resolution of 1 meter or larger (Antilla *et al.*, 2014). Terrestrial optical laser scanning offers better resolution, but even the best equipment is limited to <100m plots. First attempts have been made to increase the spatial coverage of these optical laser scanners by mounting them on snowmobiles ("mobile laser scanning") to obtain snow surface roughness data (Lacroix *et al.*, 2008; Kukko *et al.*, 2013).

Studies of the snow surface roughness can be characterized into two approaches (Antilla *et al.*, 2014). The first approach examines the effect of snow surface physical characteristics on the radiative properties of snow, which in turn affect Earth's energy budget. These studies typically use geometric roughness with correlation length (L) and root mean square height (σ) as parameters (Manninen *et al.*, 1998; Rees and Arnold, 2006). The second approach investigates the snow-atmosphere interface and its impacts on wind characteristics and the exchange of latent and sensible heat. These studies tend to use aerodynamic roughness length (Z_0) as the main variable because it is used in most models of surface-atmosphere interaction (Manes *et al.*, 2008; Gromke *et al.*, 2011). The present study falls into the second category.

Although Z_0 is a critical variable for estimating surface latent and sensible fluxes in numerical models, most land surface models treat Z_0 as a function of land cover type and usually assume it is constant over time for non-vegetated surfaces. For example, one of the more complex land surface schemes, the Community Land Model version 4.0 (CLM4), applies a

single Z_0 value of 2.4×10^{-3} m to all snow-covered surfaces. However, this is a gross simplification, as Z_0 values for snow surfaces have been reported to vary by several orders of magnitude (summarized in Brock *et al.*, 2006). Recently, the Co-Chair of the NCAR Community Climate System Model Working Group (Dr. Z.-L. Yang - U. Texas-Austin) which oversees the CLM4 development performed a modeling sensitivity study by changing aerodynamic roughness lengths in CLM4 globally. It was expected that snow sublimation and melt would increase, resulting in decreased snow water equivalent (SWE); in contrast, results showed an opposite sign change throughout the snow season. SWE was increased predominantly in boreal forest regions, and then boreal shrub regions, especially in the snow melting season. This observation shows that snow surface roughness plays an important and complicated role in the CLM4 interaction between the atmosphere, vegetation, and ground under-canopy. A deeper understanding of the way surface roughness changes with the snowpack and better methods for estimating it would improve the ability of models like CLM4 to depict hydrologic processes.

Researchers and modelers in this field have a need for a method to evaluate snow surface roughness characteristics that is relatively easy and inexpensive but improves upon the spatial coverage from plate photography without sacrificing accuracy. The present work begins to address this need. This study makes use of terrestrial laser scanning (TLS) to evaluate surface geometry and determine Z_0 on changing snow surfaces. The estimates based on surface geometry are evaluated and compared to Z_0 values calculated from field observations of wind turbulence across the snow surface.

2. BACKGROUND

The capability of a rough surface to absorb momentum from a turbulent boundary layer can be quantified by the aerodynamic roughness length. This is a measure of the vertical turbulence that occurs when a horizontal wind flows over a rough surface (Jacobsen, 2005). In general, Z_0 is a quantity that is computed from the Reynolds number and the roughness geometry of the surface. For rough turbulent regimes occurring in the atmospheric boundary layer, dependence on the Reynolds number vanishes and Z_0 is only a function of roughness geometry (Raupach *et al.*, 1991). Various relations have been found to link the geometry of roughness elements with Z_0 (e.g., Lettau, 1969; Munro 1989). The dependence of Z_0 on the size, shape, density, and distribution of surface elements has been studied using wind tunnels, analytical investigations, numerical modeling, and field observations (Grimmond and Oke, 1999; Foken, 2008). Smith (2014) provides a comprehensive review of the different approaches and models developed to analyze surface roughness. He rightly points out that almost all of the models were developed for simplistic natural surfaces (i.e. regular arrays of roughness elements). The lack of a clear formulation for calculating Z_0 as a function of surface roughness is due to the complexity of surfaces that exists in nature.

There are two approaches available to determine Z_0 for such surfaces. The most robust method for estimating Z_0 is an **anemometric** approach (Jacobson, 2005). This method relies on field observations of wind turbulence movement to generate a logarithmic wind profile and solve for aerodynamic variables, such as Z_0. The anemometric method can be used for any surface or arrangement of roughness elements, but requires a tower for wind and temperature

profile measurements that is expensive and difficult to install, operate, and maintain. In contrast, the **geometric** method uses algorithms relating Z_0 to characteristics of surface roughness elements, and thus does not require tower instrumentation but only a measure of the geometry of the surface (Lettau, 1969). This study obtained Z_0 values from anemometric measurement and used them as a baseline to evaluate geometric methods.

Anemometric data are used to determine Z_0 by creating and solving the logarithmic wind profile. This is an empirical relation to describe the vertical distribution of horizontal wind speeds within the lowest portion of the planetary boundary layer (Oke, 1987). The equation to estimate the wind speed (u in ms^{-1}) at height z (in m) above a surface is given by:

$$u_z = \frac{u_*}{k} \ln[\frac{z}{Z_0} + \psi(z, Z_0, L)] \tag{1},$$

where u_* is the friction velocity (ms^{-1}), k is the Von Kármán constant (~0.40), and ψ is a stability term where L is the Monin-Obukhov stability parameter. Under neutral stability conditions, $z/L = 0$ and ψ is not included.

The most common geometric approach is simply a function of the height of the elements:

$$Z_0 = f_0 z_h \tag{2},$$

where z_h is the mean height of roughness elements, and f_0 is an empirical coefficient derived from observation (Fassnacht *et al.*, 2015). The frontal area index (which combines mean height, breadth, and density of the roughness elements) is defined as roughness area density (λF) = L_y z_h ρ_{el}, where L_y is the mean breadth of the roughness elements perpendicular to the wind

direction and ρ_{el} is the density or number (n) of roughness elements per unit area (Raupach, 1992). Lettau (1969) developed a formula for Z_0 for irregular arrays of reasonably homogenous elements:

$$Z_0 = 0.5\ z_h\ \lambda F \qquad (3).$$

In the Lettau formula, the coefficient 0.5 represents an average drag coefficient for the roughness elements, determined experimentally. Other methods have been developed, especially to consider more regularly-shaped and distributed roughness elements, such as buildings in an urban setting (e.g., Counihan, 1971; Macdonald *et al.*, 1998). Since the roughness elements (furrows) in this study site were semi-regular, the Counihan formulation was also appropriate for use in this study, and is given as:

$$Z_0 = z_h\left(1.8\frac{A_f}{A_d} - 0.08\right) \qquad (4),$$

where A_f is the total area silhouetted by the roughness elements and A_d is the total area covered by roughness elements.

3. STUDY SITE

Data were collected during the winters of 2013-2014 and 2014-2015 at the Colorado State University Horticultural Farm experimental site east of Fort Collins, Colorado . A meteorological tower was constructed and instrumented on the east end of a 100 m by 35 m field in an area with prevailing winds from the west (Figures 1 and 2). Wind and temperature data were recorded on the meteorological tower continuously starting in February 2014. A representative wind rose in seen in Figure 3, displaying wind directions as well as the proportion of winds above the 4.0 ms^{-1} threshold described in the next section. The upwind fetch was left undisturbed for several months in the first winter, and then plowed with regular furrows orthogonal to the prevailing wind direction to induce surface roughness. The furrows spanned the entire width of the field and were approximately 40cm deep. These induced roughness elements allowed for examination of Z_0 under different surface conditions and allowed for terrain smoothing effects to be studied when snow cover was present. The surface roughness can increase or decrease during snow accumulation as the snow follows the underlying terrain in the initial stages of accumulation (Davison, 2004). During the summer after the plowing, some weeds and short crop residue grew in the field, which added additional small roughness elements to the study site (Figure 2).

Over the past century, Fort Collins, CO averaged 47 inches (120 cm) of snowfall per year. The winters of 2013-2014 and 2014-2015 were below average, with 39 and 32 inches (100 and 80 cm), respectively (<ncdc.noaa.gov>). Each winter had approximately 9 separate snowfall events, representing non-contiguous snowfall from distinct storms. Of these 18 events during

the two winters, 12 were captured by the LiDAR scanning process described above soon after

snowfall finished.

Figure 1: Terrestrial LiDAR scanner and instrumented meteorological tower at the study site.

Figure 2: Study site on January 17, 2015 showing sparse crop residue and weed vegetation.
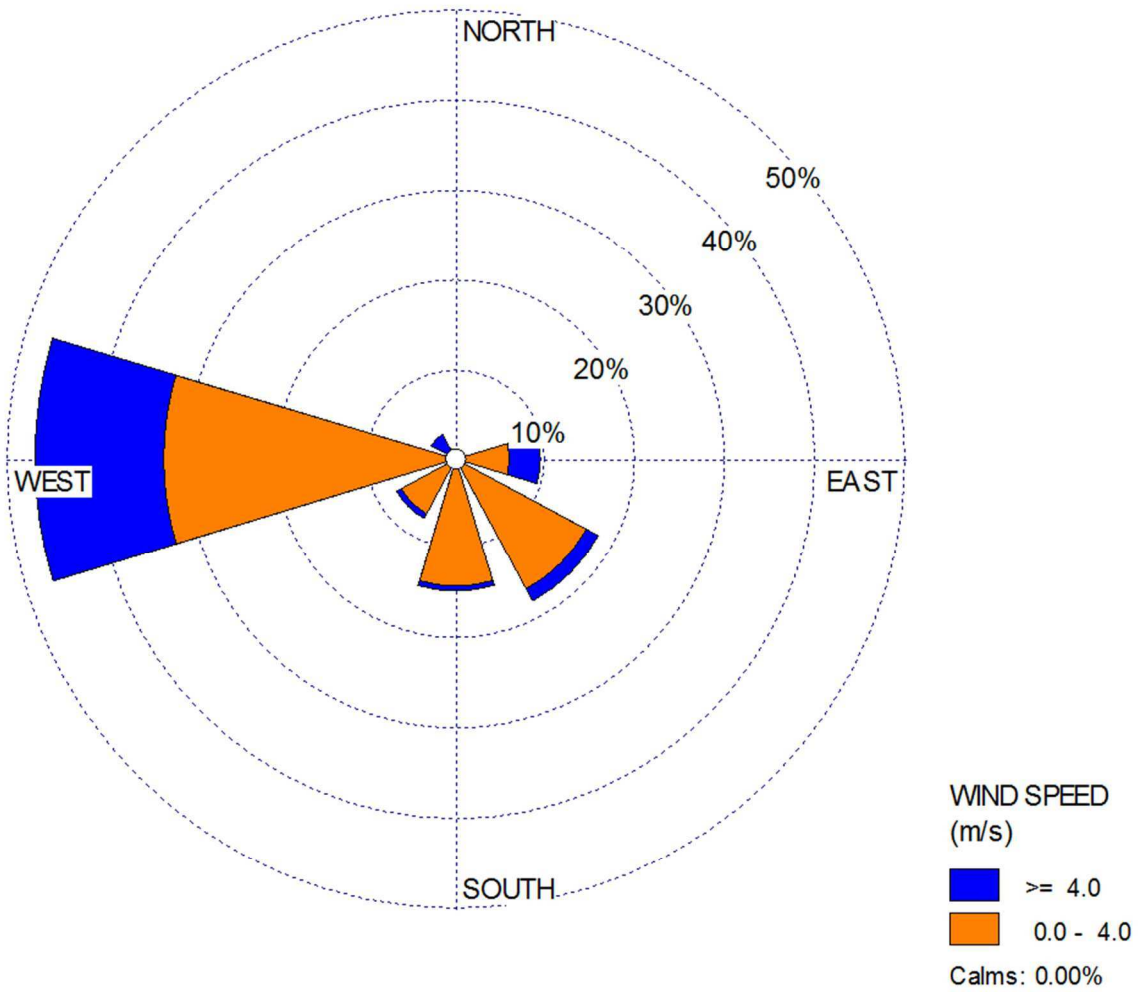
Figure 3: Wind rose from study site constructed with data from February to April of 2014. Only profiles with wind speeds above 4.0 ms^{-1} coming from the upwind fetch were considered.

4. METHODS

4.1 ANEMOMETRIC MEASUREMENT

The meteorological tower was instrumented at ten levels over a 5-m height (Figure 1). Five Davis Instruments Cup Anemometers and five Decagon Devices DS-2 Sonic Anemometers were used to capture wind profiles, sampling every second then averaging and recording every minute. Data were quality controlled per Andreas *et al.* (2006), such that only profiles with complete data, under neutral stratification, with winds coming from the upwind fetch, and with high correlation coefficients between $u_{(z)}$ and $\ln_{(z)}$ were considered. At this site, the upwind fetch was defined by measuring the angles to the upwind corners of the field from the meteorological tower. These constraints reduced the eight months of data over two winters to 153 acceptable minute-profiles.

At low wind speeds, wind turbulence is difficult to measure because the wind is often directionally inconsistent (Andreas *et al.*, 1998). Requiring wind speeds of at least 4 m s^{-1} at all levels eliminates conditions without consistent wind direction and helps ensure neutral stratification. The equations to calculate Z_0 from empirical data without using Monin-Obukhov stability terms are valid strictly for neutral stratification, which is the atmospheric condition when temperature gradients are not strong enough to allow unrestrained convection but not weak enough to prevent some convection and mixing of air parcels (Jacobson, 2005). A further test for neutral stratification was performed based on Andreas and Claffey (1995) and uses a bulk Richardson number:

$$Ri_B = \frac{R}{T_S + 273.15} \frac{(T_S - (T_2 + \gamma R))}{U_2^2} \qquad (5),$$

where R is the reference height of the mid-point anemometer on the tower (2.28m); T_2 is the

air temperature measured at the nearest anemometer, at 2.39m; U_2 is the measured wind

speed; T_s is the snow surface temperature (degrees C) estimated from the temperature profile;

and $\gamma = g/c_p$ converts T_2 to potential temperature, where c_p is the specific heat of air at

constant pressure and g is the force of gravity. In practical use, the bulk Richardson number

determines whether convection is free or forced. In the profiles that passed the screening, Ri_B

was never more than 0.03, marking these profiles as collected during near-neutral stratification

(Andreas and Claffey, 1995).

Working with top-quality equipment and five anemometers, Andreas *et al.* (2006) only

retained profiles with a correlation coefficient of r>0.99. The current study employed ten

anemometers of lower cost and accuracy, so this correlation coefficient threshold was relaxed

to r>0.95. A least squares regression fitted to these profiles (see Figure 4) of wind speed [$u_{(z)}$]

vs. natural log of measurement height [$\ln_{(z)}$] yielded slope (S) and intercept (I) which were used

to compute the aerodynamic roughness length Z_0 (Jacobson, 2005), following the equation:

$$U(z) = S \ln(z) + I \tag{6},$$

where: $$S = \frac{u_*}{k} \tag{7},$$

and: $$I = -\frac{u_*}{k}\ln(Z_0) = -S \ln(Z_0) \tag{8}.$$

The meteorological tower was also instrumented with five Decagon Devices VP-3

sensors which recorded temperature and relative humidity. These measurements are essential

for calculating sensible and latent heat fluxes from the snowpack. However, in a study such as this one focused on aerodynamic roughness length, these measurements were only used to make checks on the wind profiles. Temperature measurements were used to calculate bulk Richardson numbers as described above.

4.2 TERRESTRIAL LASER SCANNING

Terrestrial laser scanning (TLS), also known as LiDAR (light detection and ranging), was used to generate a three-dimensional point cloud of the upwind fetch being measured by the meteorological tower. The scanner used was a FARO® Focus3D X 130 model with a ranging error of ±2mm and a wavelength of 532 nm. This system measures the time between a light pulse emission and its detection, which equates to a distance between the TLS and the surface of interest (<www.faro.com/en-us/products/3d-surveying/faro-focus3d/overview#main>). Multiple scans were conducted during the winters to capture changing snow conditions, with an emphasis on scanning the site once per major snowfall event. The scanner was set up at two different locations to capture the variable topography in the field. Scans were then referenced together in the FARO Scene software (FARO Scene 5.4, 2014) using reference spheres (see Figure 1). This process yielded a cloud with non-regularly spaced points at an approximate resolution of 0.75 cm.

The present geometric methods cannot use a data point cloud and require data on a regular grid (Holland *et al.*, 2008). The data were interpolated to a 1 cm resolution with the default kriging method provided by Golden Software's Surfer 8® (Golden Software Surfer 8,

2008). Kriging was used since it is the interpolation method which yields the best linear

unbiased prediction of intermediate values between points (Isaaks and Srivastava, 1989). The

gridded data were detrended in Surfer 8 by subtracting the mean linear best-fit plane across

the x and y directions. Detrending was performed to remove bias in the analysis created from

the slope of the field or angle of the LiDAR scanner (Fassnacht *et al.*, 2009a). The grid was then

evaluated in a MathWorks MATLAB program using the Lettau and Counihan methods

(Fassnacht *et al.*, 2015) to empirically compute Z_0 based on the height and area covered by the

roughness elements.

The Nash-Sutcliffe Efficiency Coefficient (NSE) was used to assess the difference

between the Z_0 estimation methods in the form of modeled versus observed values, following

the formula:

$$E = 1 - \frac{\sum_{t=1}^{T}(X_0^t - X_m^t)^2}{\sum_{t=1}^{T}(X_0^t - \overline{X_0})^2}$$ (9),

where $\overline{Xo}$ is the mean of the observed values, X_m^t is modeled value at time t, and X_o^t is

observed value at time t. A NSE of 1 corresponds to a perfect match between modeled and

observed data, while a NSE of 0 indicates that the mean of the data is as accurate as the model

predictions, and a negative NSE indicates that the observed mean is better predictor than the

model (Nash and Sutcliffe, 1970).
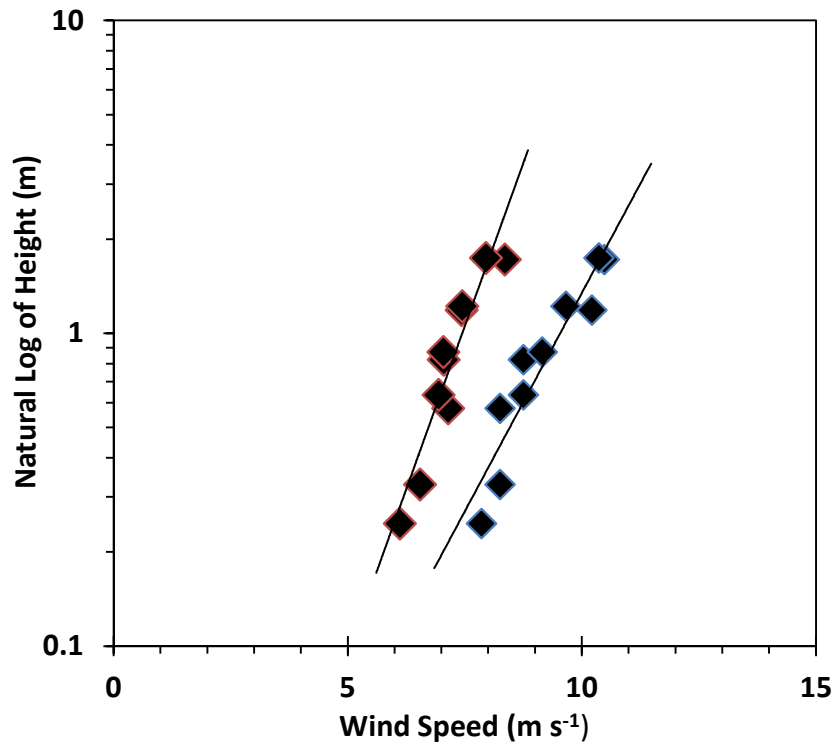
Figure 4: Two example representative logarithmic wind speed profiles that survived quality controls. Solid lines are the fits based on the least-squares regression.

5.   RESULTS

The ideal comparison of the two approaches for calculating Z_0 would be to compare the wind speed profile for the exact hour that the scan was taken to the geometric calculation. However, due to the screening process described in the methods section, only 153 acceptable profiles were available for this comparison. For 8 of the 11 scans, a profile was available on the day of the scan or on one of the days immediately before or after the scan day. A time-lapse camera mounted on the meteorological tower provided photographs of the ground surface which were used to manually estimate snow-covered area (SCA) and match the acceptable profile to the ground conditions during the scan. In the three cases when an acceptable profile was not available, the screening requirements were relaxed by considering just the five more accurate sonic anemometers in the wind speed profile. The sonic anemometers are higher quality instruments with less error than the cup anemometers, and using just those five instruments yielded a higher correlation coefficient between $u_{(z)}$ and $\ln_{(z)}$ and more profiles which passed screening as per Andres *et al.* (2006).

Table 1 displays the profile matching results, with the anemometric Z_0 shown next to the corresponding Z_0 values from the two geometric methods. The measured anemometric Z_0 values range from 0.2 to 52×10^{-3}m. The computed geometric values from the Lettau method are generally smaller than the anemometric, with a range of 0.06 to 13×10^{-3}m while the Counihan method computed generally larger Z_0 values, ranging from 3 to 41×10^{-3}m. It should be noted that the geometric values displayed are for the west to east direction, perpendicular to the furrows in the field. The study site was plowed into furrows between scan dates 3 and 4.

This induced roughness is reflected in the change in Z_0 values for all three methods. The vegetation growth over the summer is likely a factor influencing the increase in Z_0 from scans 4 and 5 to scans 6-12. More and larger roughness elements like weeds lead to increased turbulence and thus higher Z_0.

The NSE values were computed using the anemometric Z_0 as the observed data and different geometric Z_0 values as the modeled data to determine how well the geometric method matched anemometric results. For the Lettau method, the calculated NSE was 0.14, while the Counihan NSE was -1.1, indicating that the usefulness of the Counihan method is limited. These differences are seen in the scatter in Z_0 values from the Counihan method versus the anemometric method (Figure 5). Although the Lettau NSE is only 0.14, there is a correlation between the anemometric and Lettau method Z_0 values (Figure 5), and the coefficient of determination (R^2) between these data is high (0.90). In fact, with an empirically-derived adjustment factor of 2.27 added to the Lettau results, we can reach an NSE of 0.98, a near perfect match with observed anemometric data (Figure 6). It would be interesting to compare this factor across other locations and data sets to determine if a broader adjustment to the Lettau formula would make sense.

The data showed a strong response from Z_0 to changing snow cover (Figure 7). The correlation between Z_0 and SCA for both the anemometric and Lettau methods showed coefficients of determination greater than 0.7 (Figure 6). The Z_0 values computed with the Counihan formulation were not correlated to snow-covered area ($R^2 = 0.01$).

18

Figures 8 and 9 show the range and distribution of Z_0 from all of the anemometric

profiles, not just the ones matched with laser scans. These again reflect the large change in Z_0

when the field is plowed, and they also showcase the variability over the season as snow cover

and vegetation change.

Table 1: Comparison of Z_0 values across different methods during the winters of 2013-2014 and 2014-2015. Note: * indicates unplowed field without furrows to induce roughness

Scan Number	Scan date	Anemometric Z_0 (x 10^{-3} m)	Lettau Z_0 (x 10^{-3} m)	Counihan Z_0 (x 10^{-3} m)	Snow Covered Area (%)
1*	2/13/2014	0.7	0.06	3	0
2*	2/26/2014	0.6	0.4	9	100
3*	3/3/2014	0.8	0.6	8	30
4	3/22/2014	2.5	1.4	30	100
5	4/13/2014	8.9	2.1	16	70
6	11/14/2014	13	4.5	39	70
7	12/28/2015	18	8.7	19	50
8	1/17/2015	32	13	41	0
9	2/21/2015	20	11	28	10
10	2/24/2015	16	4.1	21	100
11	2/28/2015	19	9.8	10	30
12	3/5/2015	9	3.3	30	90
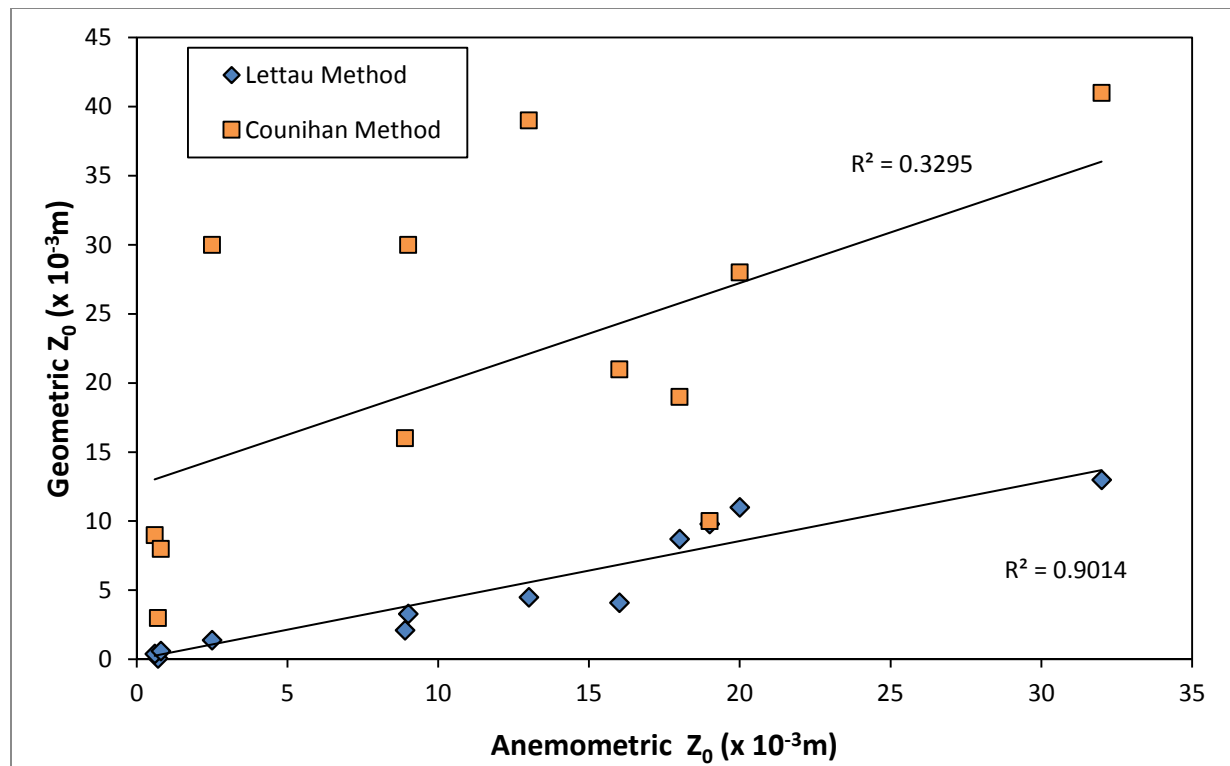
Figure 5: Comparison of Lettau and Counihan geometric methods to the anemometric method.
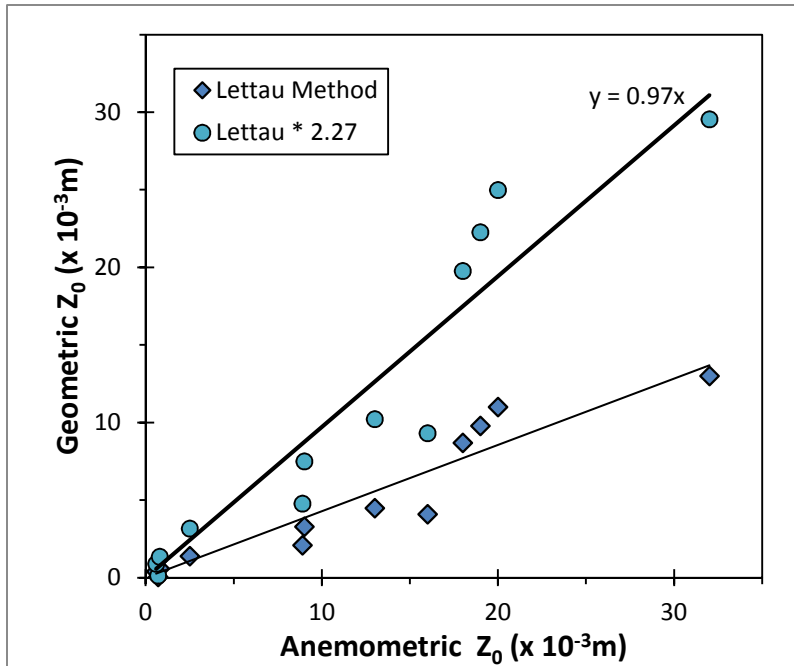
Figure 6: Lettau method with a simple adjustment factor of 2.27 matches much closer to 1:1 with the observed anemometric data.
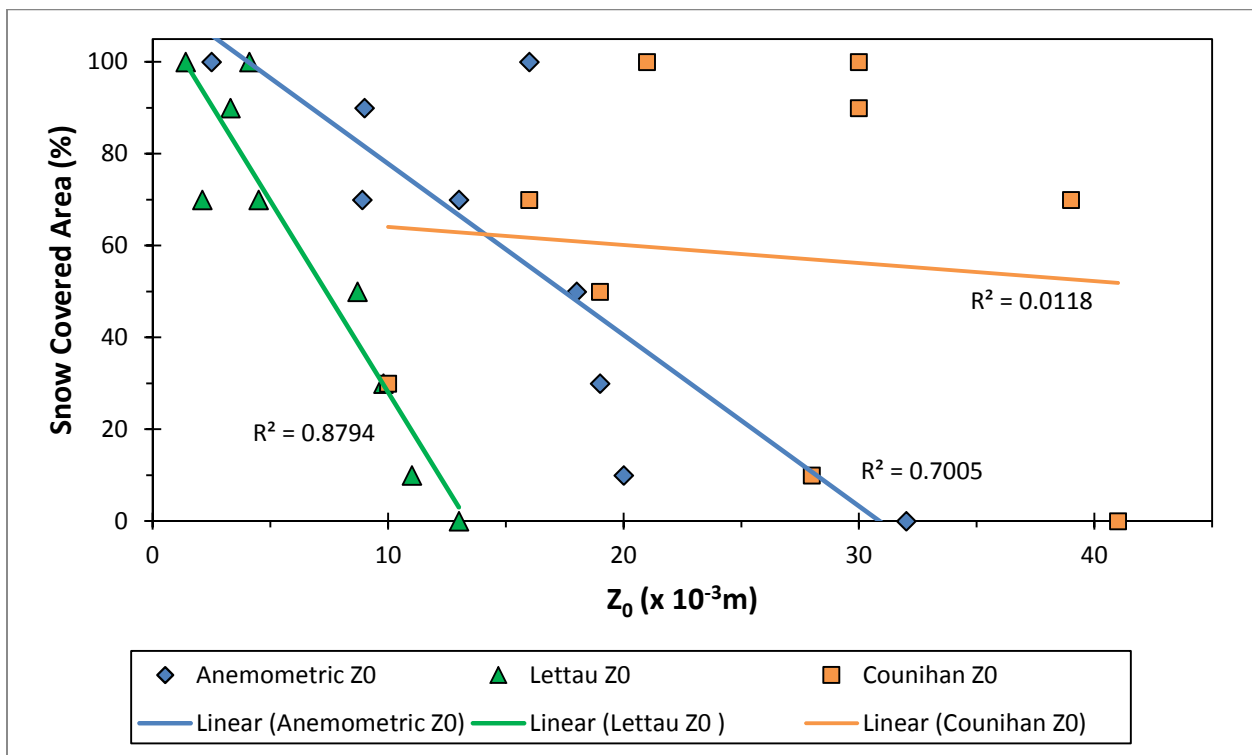
Figure 7: Z_0 plotted against snow covered area for all of the scans (4-12) on the plowed field.
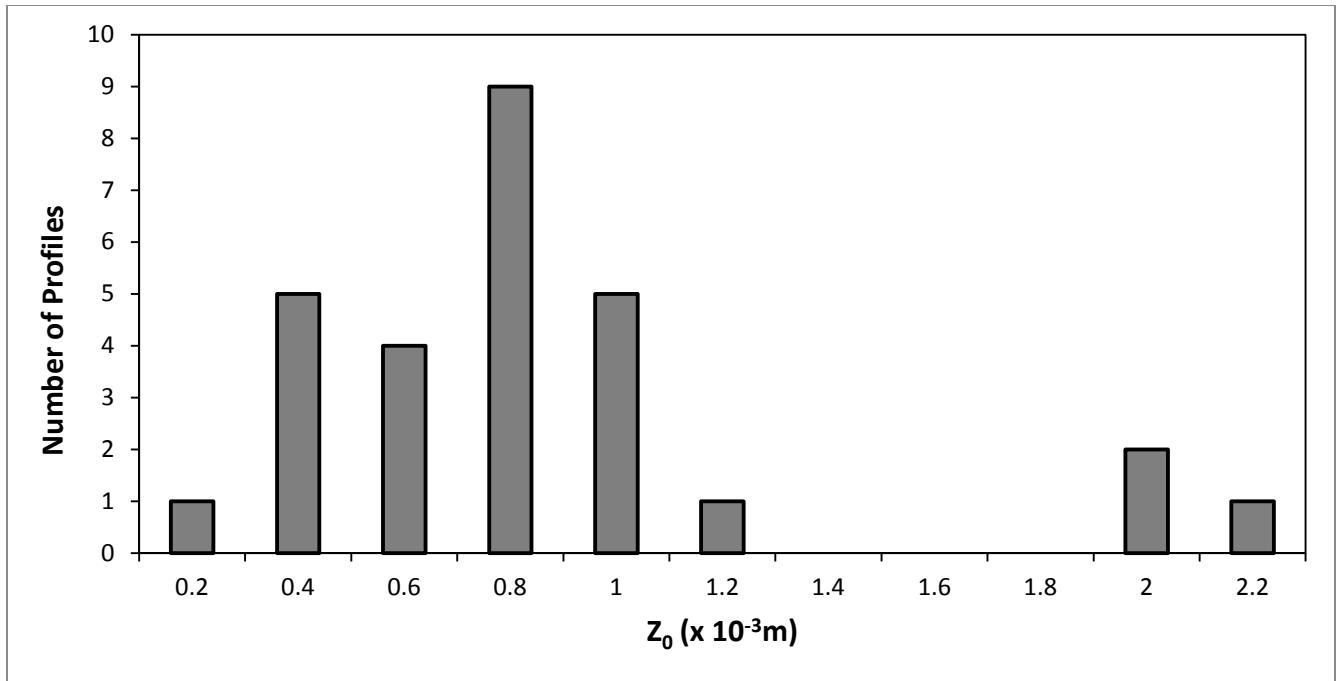
Figure 8: Histogram showing range and distribution of Z_0 values for the unplowed field from anemometric data (28 wind-speed profiles). The mean for this data is 0.8×10^{-3} m, with a standard deviation of 0.5×10^{-3} m. The median is 0.7×10^{-3} m, skew is 1.6 and kurtosis is 2.4.
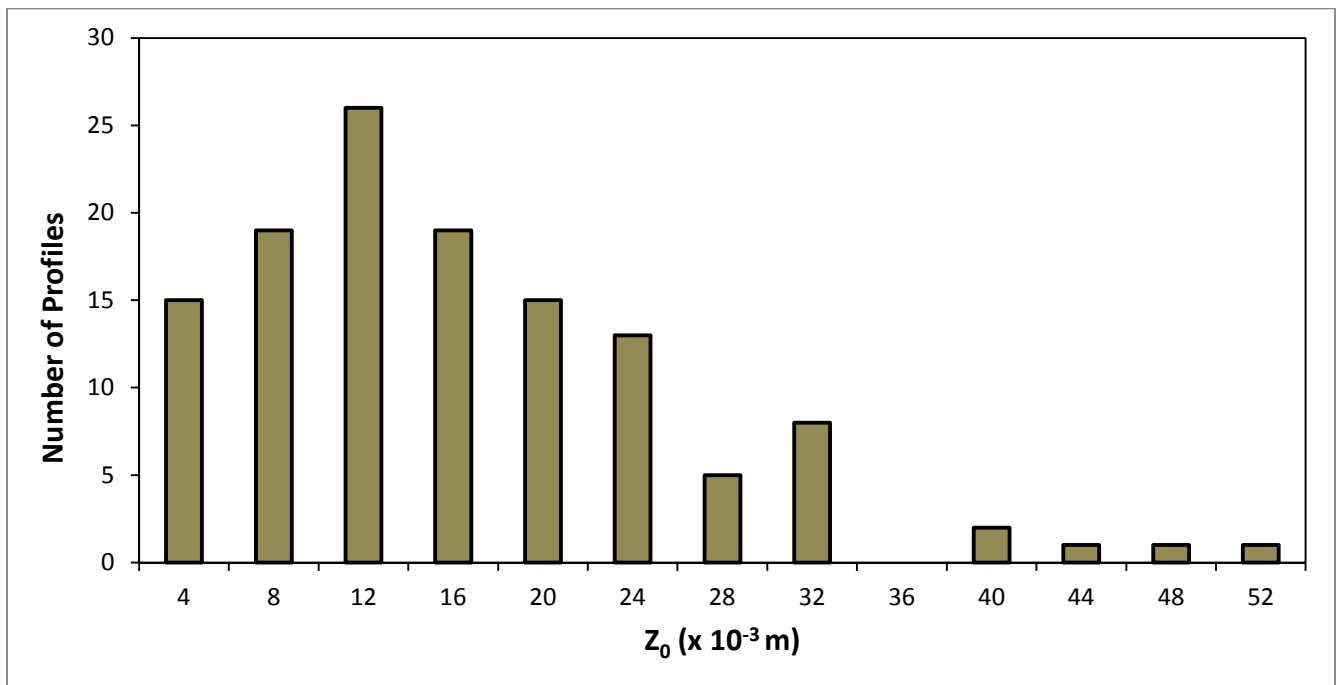
Figure 9: Histogram showing range and distribution of Z_0 values for the plowed field from anemometric data (125 wind-speed profiles). The mean for this data is 15×10^{-3} m, with a standard deviation of 9.5×10^{-3} m. The median is 13×10^{-3} m, skew is 1.1 and kurtosis is 1.6.

6.   DISCUSSION

Z_0 values for snow surfaces have been reported to vary by several orders of magnitude (summarized in Brock *et al.*, 2006), so the range of values seen in Table 1 is not atypical. Brock *et al.* (2006) reviewed published studies on snow surfaces and reported a range of Z_0 values ranging from 0.2 to 30 $x10^{-3}$ m. The higher Z_0 values in this literature are from studies of ablation hollows (14 $x10^{-3}$ m) and snow penitentes (30 $x10^{-3}$ m). These natural roughness elements provide a good comparison for the furrows added to this study site. The mean anemometric Z_0 for the plowed field was 15 $x10^{-3}$ m (Figure 9), while the means for the Lettau and Counihan methods were 6.4 $x10^{-3}$ m and 26 $x10^{-3}$ m, respectively (Table 1). The anemometric Z_0 values observed by this study on the flat field (mean of 0.8 $x10^{-3}$m, Figure 8) are in agreement with the values reported in Brock *et al.* (2006) for fresh snow and glacier snow (0.2 to 0.9 $x10^{-3}$m).

There can be an order of magnitude difference in the geometric Z_0 due in part to the limitations of the Lettau method. The Lettau method "*works well when roughness elements are fairly isolated*" (Businger, 1975). However, this site featured roughness elements (furrows) which were regular and connected, which is not the ideal scenario for the Lettau formulation. This helps explain some of the differences between the Lettau and the anemometric results. In every case, the Lettau method underestimates Z_0 compared to the anemometric method, often by a factor of 2 or 3. On the other hand, the Counihan method tends to overestimate Z_0 compared to the anemometric method. This is particularly true with the unplowed (flat) field.

Since the Counihan method is best with ordered and regular roughness elements, it overestimates Z_0 on the flat field without any obstructions.

There are potential errors related to the geometric methods, including data acquisition and processing. One question is does the scan actually provide a good representation of the surface of the field? Trial efforts used only one scan centered in the upwind fetch, but the coverage was much improved by using two scans offset on either side of the field. When referenced together, these scans eliminated most of the topographic shadows and captured more of the variation in the field due to the presence of furrows. With more scans, there are more points, and thus greater resolution in the areas closest to the LiDAR scanner, while areas further away are less well represented with coarser resolution. Studies performed using a similar TLS unit to generate gridded point maps found a mean absolute error in point accuracy of less than 1 mm over a distance of 8 m (Revuelto *et al.*, 2014; López-Moreno *et al.*, 2015). However, topographic shadows from the furrows and small vegetation led to some features being less well-represented by the point cloud. In general, the combination of a small scan area and multiple scan locations allowed for an accurate representation of the surface, but there are still more points clustered around the scanner locations, possibly leading to issues related to interpolation.

Interpolating these points onto a regular grid with kriging allows for analysis with the Lettau and Counihan methods, but errors can still exist in interpolation due to the uneven distribution of points. The weights used during the kriging interpolation are usually based on the distance of each point from the target location, with a consideration of anisotropy in the

data (Stein *et al*., 2002). Areas on the grid with more points to average will yield a more accurate representation of the surface than areas further from the TLS unit.

This study uses the anemometric method as the empirical "true" Z_0 to evaluate the geometric methods. However, the anemometric method to estimate Z_0 from profiles of wind speed also has potential errors, in particular the specification of a zero-reference level (Z) and measurement errors. Large ranges of Z_0 values have been reported over similar surfaces (Inoue, 1989; Brock *et al.,* 2006). The frequency distribution of anemometric Z_0 values at this site shows fairly clustered values, but on both plowed and unplowed fields Z_0 values vary by an order of magnitude (Figures 8 and 9). Establishing a zero-reference level to determine measurement heights can be difficult on rough surfaces (Munro, 1989; Smith, 2014), such as this study site where the base of the anemometric tower does not correspond exactly to the troughs (base) of the roughness elements. Further snowpack accumulation and ablation (e.g., Figure 6), while fairly insignificant at this site, can also lead to significant changes in reference heights which must be taken into account.

There are also error associated with the sensors and measurement. A mix of sonic and cup anemometers was used due to financial constraints; these sensors use different measurement principles and thus may respond differently to the same wind conditions. The DS-2 sonic anemometers report an accuracy of 0.30 ms^{-1} while the Davis cup anemometers only claim accuracy of ±5% on wind speed observations. Sensors were calibrated under laboratory conditions, but a complete set of the better-performing sonic anemometers may have yielded more accurate results. Over the 153 wind profiles, the cup anemometers reported wind speeds

on average 6% lower than the 2-D sonic anemometers. Similar work performed by Edgar

Andreas and others on Ice Station Weddell (Andreas *et al.,* 2006) using higher-quality Applied

Technologies K-style 3-D anemometers were only analyze wind speed profiles with correlation

between the $U(z)$ and $\ln(z)$ of r>0.99, while this work had to relax that requirement to r>0.95 to

yield enough profiles.

The physical arrangement of the site may yield other issues. Only profiles with wind

coming from the upwind fetch were considered, so any roughness elements on the sides of the

field should not be relevant and thus not used. However, half of the field does have an

approximately 3m tall dense juniper hedge located 10m upwind of the western end of the field.

The rule of thumb is that an anemometer is affected by an area approximately 20 times its

height (Andreas, *pers. comm.*, 2014). The highest anemometer on the tower was mounted at

4.25m, giving it an effective range of 85m. The hedge row is located just outside this range, but

it is still possible that it had some effects on the wind profiles. A site without any such

obstructions would have been the most ideal for this analysis, but such sites are often in

remote polar regions with limited accessibility.

The data also showed a strong response from Z_0 to changing snow cover (Figure 7).

From a broad theoretical perspective, complete snow cover should lead to less rough surfaces

(lower Z_0) because of the tendency for snowfall to fill in surface depressions and thus smooth

out roughness elements (Veitinger *et al.*, 2013). This is especially true in windy conditions

where snow is redistributed. The relation between Z_0 and snow covered area is complicated

due to many other factors like snowpack metamorphism and wind redistribution that affect the

roughness of the snow surface (Gromke *et al.*, 2011; Anttila *et al.,* 2014). For example, scans 4 and 10 both were conducted during 100% SCA with similar snow depths of ~20 cm, but they yielded different Z_0 values. At this study site, the furrows were the major roughness elements, and more snow tended to reduce the effects of the furrows on Z_0. Snow depth was thus a significant factor at this site, because larger snowfalls filled in a larger part of the troughs and left a smoother overall surface, particularly if wind had time to redistribute snow from the peaks into the valleys of the field. Schweizer *et al.* (2003) stated that a snow depth of 0.3 to 1m is required to eliminate terrain roughness. There was never enough snowfall at this site to completely fill the troughs and smooth the entire surface. However, the Z_0 values would vary much less with snow accumulation deep enough to fully bury the troughs (see Veitinger *et al.*, 2013 for more on terrain smoothing and snow roughness). Despite these additional influencing factors, the correlation between Z_0 and SCA for both the anemometric and Lettau methods was high with coefficients of determination greater than 0.7 (Figure 7). The Z_0 values computed with the Counihan formulation were much less correlated to SCA, perhaps since this method was formulated for urban, regular elements.

The failure of the Counihan method, perhaps because of the physical setting, brings up the question of the larger relevance of this work. This study was carried out on an agricultural field with very short vegetation. As such, it is relevant to many similar landscapes across the world: farms, fields, steppes, and rangelands. However, to apply these methods to a forested area or an urban landscape would require a different set of tools and techniques, and is certainly a ripe area for future research.

An objective of this work was to test a simple method for determining aerodynamic Z_0 without the requirements of the anemometric method, i.e., a method that is more versatile to implement. Instrumenting a meteorological tower for this work and accumulating sufficient data is an expensive and time-consuming process. There exists high demand for more accurate and widespread estimations of Z_0 for use in hydrological, climate, and other models. Therefore, methods that do not rely on meteorological towers but have similar efficacy are called for to advance knowledge in this field. The terrestrial LiDAR system used for this work is one step toward a more mobile and robust system for determining Z_0. This particular device is very accurate at short distances and, combined with the geometric analysis, provides a good method to estimate Z_0 on a small scale surface, such as an agricultural field. However, the system demonstrated in this study could not easily be scaled up to calculate Z_0 in a larger area. Other methods such as airborne LiDAR or long-range TLS units will need to be put into use. Various larger extent airborne LiDAR datasets now exist (e.g., <*opentopography.org*>). Recent advances in surveying are rapidly improving the resolution, extent, and availability of topographic datasets. There is great potential to expand this analysis to a larger scale using these datasets which allow for geometric characterizations.

7. CONCLUSIONS

This study explored the use of geometric methods and terrestrial LiDAR to estimate aerodynamic roughness length of a study plot with changing surface conditions and snow cover. Both the Lettau and Counihan formulations were used to evaluate surface geometry. These estimations were compared to Z_0 values calculated from field observations of wind turbulence across the surface of the study site. The results showed a strong response from both geometric methods and the anemometric method when the study site was plowed to induce roughness. Further, both the Lettau method and the anemometric method Z_0 results were well-correlated with changing snow cover. The coefficient of determination between Z_0 and snow-covered area for both methods was greater than 0.7. In direct comparison to the measured anemometric results, the Lettau method Z_0 values had a Nash-Sutcliffe Efficiency Coefficient of 0.14, but a strong coefficient of determination ($R^2 = 0.90$). The Counihan method yielded less accurate results compared to the anemometric data, with a NSE of -1.1. The success with the Lettau method for evaluating surface geometry and correlating with anemometric observations is encouraging for future work in this field. Further analysis is still needed to examine more complicated geometric metrics or merge them to yield better approximations. Further work should focus on expanding this methodology for use with larger spatial scales and different types of laser scanning and remote sensing technology.

8. REFERENCES

Andreas, E.L., 1987: A theory for the scalar roughness and the scalar transfer coefficients over snow and sea ice. *Boundary-Layer Meteorology* 38, 159–184.

Andreas, E.L, K.J. Claffey, R.E. Jordan, C.W. Fairall, P.S. Guest, P.O.G. Persson, A.A. Grachev., 2006: Evaluations of the von Karman constant in the atmospheric surface layer. *Journal of Fluid Mechanics,* 559, 117-149.

Andreas, E.L., P.O.G. Persson, R.E. Jordan, T.W. Horst, P.S. Guest, A.A. Grachev, C.W. Fairall, 2010: Parameterizing turbulent exchange over sea ice in winter. *Journal of Hydrometeorol*ogy, 11, 87–104.

Andreas, E.L, 2011: A relationship between the aerodynamic and physical roughness of winter sea ice. *Quarterly Journal of the Royal Meteorological Society*, 137, 1581-1588.

Anttila, K., T. Manninen, T. Karjalainen, P. Lahtinen, A. Riihelä, N. Siljamo, 2014: The temporal and spatial variability in submeter scale surface roughness of seasonal snow in Sodankylä Finnish Lapland in 2009-2010. *Journal of Geophysical Research: Atmospheres, 119,* 9236-9252.

Brock, B.W., I.C. Willis, M.J. Sharp, 2006: Measurement and parameterization of aerodynamic roughness length variations at Haut Glacier d'Arolla, Switzerland. *Journal of Glaciology*, 52(177), 281-298.

Chen, X.Z., Y. Li, Y.X. Su, L.S. Han, J.S. Liao, S.B. Yang, 2014: Mapping global surface roughness using AMSR-E passive microwave remote sensing. *Geoderma* 235-236, 308-315.

Counihan, J., 1971: Wind tunnel determination of the roughness length as a function of the fetch and roughness density of three dimensional roughness elements. *Atmospheric Environment*, 5, 637-642.

Davison, B.J., 2004: *Snow accumulation in a distributed hydrological model*. Unpublished M.A.Sc. Thesis, Civil Engineering, University of Waterloo, Canada, 108pp + appendices.

Deems, J.S., S.R. Fassnacht, K.J. Elder, 2006: Fractal distribution of snow depth from LiDAR data. *Journal of Hydrometeorology*, 7(2), 285-297.

Deems, J.S., T.H. Painter, and D.C. Finnegan, 2013: Lidar measurement of snow depth: a review. *Journal of Glaciology*, 59(215), 467-479.

Fassnacht, S.R., M.W. Williams, M.V. Corrao, 2009a: Changes in the surface roughness of snow from millimetre to metre scales. *Ecological Complexity*, 6(3), 221-229.

Fassnacht, S.R., J.D. Stednick, J.S. Deems, M.V. Corrao, 2009b: Metrics for assessing snow surface roughness from digital imagery. *Water Resources Research*, 45, W00D31.

Fassnacht, S.R., 2010: Temporal changes in small scale snowpack surface roughness length for sublimation estimates in hydrological modeling. *Journal of Geographical Research*, 36(1), 43-57.

Fassnacht, S.R., I. Oprea, P.D. Shipman, J. Kirkpatrick, G. Borleske, F. Motta, D.J. Kamin, 2015: Geometric methods in the study of snow surface roughness. *Proceedings of the 35th Annual American Geophysical Union Hydrology Days*, Fort Collins, CO, p41-50.

Garratt, J.R., 1992. *The Atmospheric Boundary Layer*. Cambridge: Cambridge University Press.

Gromke, C., C. Manes, B. Walter, M. Lehning, M. Guala, 2011: Aerodynamic roughness length of fresh snow. *Boundary-Layer Meteorology,* 141, 21-34.

Holland, D.E., J.A. Berglund, J.P. Spruce, R.D. McKellip, 2008: Derivation of effective aerodynamic surface roughness in urban areas from airborne lidar terrain data. *Journal of Applied Meteorology and Climatology*, 47, 2614-2625.

Hong, S., 2010: Detection of small-scale roughness and refractive index of sea ice in passive satellite microwave remote sensing. *Remote Sensing of Environment,* 1136-1140.

Isaaks, E.H., R.M. Srivastava, 1989: *Introduction to Applied Geostatistics*. New York: Oxford University Press, 592p.

Jacobson, M.Z., 2005: *Fundamentals of Atmospheric Modeling*. Cambridge: Cambridge University Press, 813p.

Kukko, A., K. Anttila, T. Manninen, S. Kaasalainen, H. Kaartinen., 2013: Snow surface roughness from mobile laser scanning data. *Cold Regions Science and Technology* 96, 23-35.

Lacroix, P., B. Legrésy, K. Langley, S. Hamran, J. Kohler, S. Roques, F. Rémy, M. Dechambre, 2008: Instruments and Methods: In situ measurements of snow surface roughness using a laser profiler. *Journal of Glaciology 54,* 753-62.

López-Moreno, J. I., J. Revuelto, S.R. Fassnacht, C. Azorín-Molina, S. M. Vicente-Serrano, E. Morán-Tejeda, G.A. Sexstone, 2015: Snowpack variability across various spatio-temporal resolutions. *Hydrological Processes* 29, 1213-1224.

Lettau, H., 1969: Note on aerodynamic roughness-parameter estimation on the basis of roughness-element description. *Journal of Applied Meteorology*, 8, 828-832.

Macdonald, R.W., R.F. Griffiths, D.J. Hall, 1998: An improved method for the estimation of surface roughness of obstacle arrays. *Atmosphere and Environment* 32, 1857–1864.

Manes, C., M. Guala, H. Löwe, S. Bartlett, L. Egli, M. Lehning, 2008: Statistical properties of fresh snow roughness. *Water Resources Research,* 44.

Manninen, T., K. Antilla, T. Karjalainen, P. Lahtinen, 2012: Instruments and Methods - Automatic snow surface roughness estimation using digital photos. *Journal of Glaciology*, 58, 211.

Munro, D.S., 1989: Surface roughness and bulk heat transfer on a glacier: Comparison with eddy correlation. *Journal of Glaciology*, 35, 343-348.

National Climatic Data Center Web Site. www.ncdc.noaa.gov. Accessed April, 2015.

Raupach, M. R., 1992: Drag and drag partition on rough surfaces, *Boundary Layer Meteorology*, 60, 375–395.

Rees, W.G., N.S. Arnold, 2006: Scale-dependent roughness of a glacier surface: implications for radar backscatter and aerodynamic roughness modelling. *Journal of Glaciology,* 52, 214–222.

Revuelto J., J.I. López-Moreno, C. Azorin-Molina, J. Zabalza, G. Arguedas, S.M. Vicente-Serrano, 2014: Mapping the annual evolution of snow depth in a small catchment in the Pyrenees using the long-range terrestrial laser scanning. *Journal of Maps* 10, 3, 379-393.

Schweizer, J.,J. B. Jamieson, M. Schneebeli, 2003: Snow avalanche formation. *Review of Geophysics* 41, 1016.

Smith, M.W., 2014. Roughness in the earth sciences. *Earth-Science Reviews*, 136, 202-225.

Stein, A., F. Van der Meer, B. Gorte, 2002: *Spatial Statistics for Remote Sensing.* Springer Netherlands, 284p.

Veitinger, J., B. Sovilla, R.S. Purves, 2014: Influence of snow depth distribution on surface roughness in alpine terrain: A multi-scale approach. *The Cryosphere* 8, 547-69.